Optimization of long-range BOTDA sensors with high resolution using first-order bi-directional Raman amplification

Marcelo A. Soto, Gabriele Bolognini,* and Fabrizio Di Pasquale

Scuola Superiore Sant'Anna, via G. Moruzzi 1, 56124 Pisa, Italy
**g.bolognini@sssup.it*

Abstract: In this paper we perform an optimization of Brillouin optical time-domain analysis (BOTDA) sensors for achieving high resolution over long sensing ranges using distributed Raman amplification. By employing an optimized first-order bi-directional Raman amplification scheme and combining high-power fiber-Raman lasers and Fabry-Pérot lasers with low relative-intensity-noise (RIN), we demonstrate distributed sensing over 120 km of standard single-mode fiber with 2 meter spatial resolution and with a strain/temperature accuracy of 45με/2.1°C respectively.

OCIS codes: (060.2370) Fiber optics sensors; (290.5900) Scattering, stimulated Brillouin; (060.4370) Nonlinear optics, fibers.

References and links

1. M. Niklès, L. Thévenaz, and P. A. Robert, "Simple distributed fiber sensor based on Brillouin gain spectrum analysis," Opt. Lett. **21**(10), 758–760 (1996).
2. M. A. Soto, G. Bolognini, F. Di Pasquale, and L. Thévenaz, "Simplex-coded BOTDA fiber sensor with 1 m spatial resolution over a 50 km range," Opt. Lett. **35**(2), 259–261 (2010).
3. F. Rodríguez-Barrios, S. Martín-López, A. Carrasco-Sanz, P. Corredera, J. D. Ania-Castañón, L. Thévenaz, and M. González-Herráez, "Distributed Brillouin fiber sensor assisted by first-order Raman amplification," J. Lightwave Technol. **28**(15), 2162–2172 (2010).
4. S. Martín-Lopez, M. Alcon-Camas, F. Rodríguez, P. Corredera, J. D. Ania-Castañon, L. Thévenaz, and M. González-Herraez, "Brillouin optical time-domain analysis assisted by second-order Raman amplification," Opt. Express **18**(18), 18769–18778 (2010).
5. X.-H. Jia, Y.-J. Rao, L. Chang, C. Zhang, and Z.-L. Ran, "Enhanced sensing performance in long distance Brillouin optical time-domain analyzer based on Raman amplification: theoretical and experimental investigation," J. Lightwave Technol. **28**(11), 1624–1630 (2010).
6. M. N. Alahbabi, Y. T. Cho, and T. P. Newson, "150-km-range distributed temperature sensor based on coherent detection of spontaneous Brillouin backscatter and in-line Raman amplification," J. Opt. Soc. Am. B **22**(6), 1321–1324 (2005).
7. C. R. S. Fludger, V. Handerek, and R. J. Mears, "Pump to signal RIN transfer in Raman fiber amplifiers," J. Lightwave Technol. **19**(8), 1140–1148 (2001).
8. D. Alasia, M. González Herráez, L. Abrardi, S. Martin-López, and L. Thévenaz, "Detrimental effect of modulation instability on distributed optical fiber sensors using stimulated Brillouin scattering," Proc. SPIE **5855**, 587–590 (2005).
9. S. M. Foaleng, F. Rodríguez, S. Martín López, M. González Herráez, and L. Thévenaz, "Impact of self phase modulation on the performance of Brillouin distributed fibre sensors," Proc. SPIE **7653**, 76532U, 76532U-5 (2010).
10. A. Minardo, R. Bernini, L. Zeni, L. Thévenaz, and F. Briffod, "A reconstruction technique for long-range stimulated Brillouin scattering distributed fibre-optic sensors: experimental results," Meas. Sci. Technol. **16**(4), 900–908 (2005).
11. A. Minardo, R. Bernini, and L. Zeni, "A simple technique for reducing pump depletion in long-range distributed Brillouin fiber sensors," IEEE Sens. J. **9**(6), 633–634 (2009).
12. R. W. Boyd, *Nonlinear Optics*, 3rd ed. (Academic Press, 2008), Chap. 9.
13. A. Fellay, L. Thévenaz, M. Facchini, M. Nikles, and P. Robert, "Distributed sensing using stimulated Brillouin scattering: towards ultimate resolution," in *12th International Conference on Optical Fibre Sensors. Technical Digest.*, 324–327, (1997).
14. S. Faralli, and F. Di Pasquale, "Impact of double Rayleigh scattering noise in distributed higher order Raman pumping schemes," IEEE Photon. Technol. Lett. **15**(6), 804–806 (2003).
15. M. N. Islam, *Raman Amplifiers for Telecommunications 1* (Springer-Verlag, 2004).
16. V. E. Perlin, and H. G. Winful, "Optimizing the Noise Performance of Broad-Band WDM Systems With Distributed Raman Amplification," IEEE Photon. Technol. Lett. **14**(8), 1199–1201 (2002).

#139361 - $15.00 USD Received 8 Dec 2010; revised 20 Jan 2011; accepted 20 Jan 2011; published 23 Feb 2011

17. S. Faralli, G. Bolognini, M. A. Andrade, and F. Di Pasquale, "Unrepeated WDM Transmission systems based on advanced first-order and higher order Raman-copumping technologies," J. Lightwave Technol. **25**(11), 3519–3527 (2007).
18. J. Zhou, J. Chen, Y. Jaouën, L. Yi, X. Li, H. Petit, and P. Gallion, "A new frequency model for pump-to-signal RIN transfer in Brillouin fiber amplifiers," IEEE Photon. Technol. Lett. **19**(13), 978–980 (2007).
19. J. Zhou, L. Yi, Y. Jaouën, J. Chen, and P. Gallion, "Pump-to-Stokes relative intensity noise transfer in Brillouin amplifiers," in *Proceedings of 33rd European Conference and Exhibition of Optical Communication* (ECOC), Berlin, Germany (2007), paper 2.4.3.

1. Introduction

Distributed optical fiber sensors technology is attracting a growing interest thanks to its wide range of potential industrial applications in strategic sectors such as energy, security, defense and transportation, among others. In particular, fiber sensors based on Brillouin optical time-domain analysis (BOTDA) exploit the dependence of the Brillouin frequency shift (BFS) parameter on strain and temperature [1–3], allowing for highly accurate distributed measurements over long single-mode fibers (SMF) exceeding several tens of kilometers, especially relevant for civil and industrial infrastructure monitoring. An important field of investigation related to BOTDA deals with the possibility of attaining longer sensing distances [2–5], and several innovative approaches have been recently proposed addressing this matter. In particular, the measurement ranges of standard BOTDA systems have been sensibly enhanced by the use of pulse coding [2] and the use of distributed Raman amplification [3–5].

In this paper we analyze the impact of distributed Raman amplification, performing a careful optimization (employing both numerical models and experiments) which is crucial for a significant sensing range enhancement, allowing one to fully exploit the Raman amplification benefits and minimize at the same time the potential penalties coming from several sources of noise. In fact, although distributed Raman amplification can be used for enhancing the performance of distributed fiber sensors based on stimulated or spontaneous Brillouin scattering [3–6], a great care must be taken in their practical implementation. Actually, three main sources of distortions have been observed or can be expected in Raman-assisted BOTDA sensors, potentially affecting their performance to a great extent: RIN transfer from the Raman pumps to the continuous-wave (CW) Brillouin probe [3,7], fiber nonlinear effects [8,9] and nonlocal effects induced by pump depletion [10,11]. In order to fully exploit the Raman amplification benefit, it is then necessary to minimize such arising penalties by employing suitable techniques and devising effective solutions.

In this paper, we have carried out a thorough numerical analysis in order to optimize the BOTDA system parameters and decrease the impact of the above-mentioned penalties. The optimization has been performed considering the optical signal-to-noise ratio (OSNR) of the probe signal, the minimum power difference between Brillouin pump and probe (to avoid pump depletion [10,11]) and the maximum Brillouin pump power along the sensing fiber (to avoid nonlinear effects [8,9]). We theoretically show and experimentally verify that, when employing Raman pumps in co-propagating direction with respect to the CW-probe, low relative intensity-noise (RIN) lasers are crucial in avoiding strong noise transfer effect and the consequent strong induced penalties. Actually, we experimentally attain high-accuracy distributed measurements over 120 km of SMF using optimized first-order bi-directional Raman amplification. The performed system optimization, together with the skillful combination of high-power fiber Raman lasers (FRL) and low-RIN polarization-multiplexed Fabry-Pérot (FP) lasers, allows us to achieve 2-m spatial resolution throughout the fiber length and (worst-case) strain/temperature resolutions of 45με/2.1°C respectively.

2. Theoretical background of BOTDA sensors

Stimulated Brillouin scattering (SBS) in optical fibers can be classically described as a nonlinear interaction between two counter-propagating optical waves and an acoustic wave [12]. In BOTDA sensors, a strong pulsed pump wave (whose pulse duration determines the spatial resolution of the sensor) and a weak counter-propagating CW probe signal interact

#139361 - $15.00 USD Received 8 Dec 2010; revised 20 Jan 2011; accepted 20 Jan 2011; published 23 Feb 2011

with acoustic phonons in the fiber through SBS, leading to an energy exchange among the optical waves. This energy transfer takes place at any fiber position whenever the optical waves spatially overlap inside the fiber and the frequency difference is within the local Brillouin gain spectrum (BGS). Actually, the maximum amplification occurs when the frequency offset between the two optical waves equals the peak acoustic frequency, i.e. at the BFS of the fiber [10]. Thus, the strain and temperature dependence of the BFS provides an effective mechanism to perform distributed sensing along an optical fiber [1,2].

There are basically two types of configurations for BOTDA sensors; namely Brillouin gain and Brillouin loss configurations. In the first case, the probe signal is downshifted in frequency with respect to the pump wave, so that the pump pulse amplifies the probe signal. However, in the second case (Brillouin loss configuration), the probe signal is frequency-upshifted with respect to the pump wave, resulting in depletion of the probe signal as a consequence of the SBS interaction.

By sweeping the frequency difference between the two counter-propagating optical signals ($\Delta\nu$) and measuring the power variations of the probe signal (ΔI_{CW}), the BGS can be obtained (and hence the BFS of the fiber) as a function of the distance [1], with a spatial resolution which is equal to the SBS interaction length (i.e. half of the pump pulse length [10]). Temporal changes in the CW probe intensity (ΔI_{CW}) can be measured as a function of time t and $\Delta\nu$ at the near fiber-end ($z = 0$), resulting in:

$$\Delta I_{CW}(t,\Delta\nu) = I_{CWL}\exp(-\alpha L)\left\{\exp\left[\int_{\upsilon_g t/2+\Delta z}^{\upsilon_g t/2} -g_B(\xi,\Delta\nu)Ip(\xi,\Delta\nu)d\xi\right]-1\right\}, \quad (1)$$

with $0 < t < 2(L-\Delta z)/\upsilon_g$ [10]; where L is the fiber length, v_g is the group velocity, Δz is the spatial resolution, I_{CWL} is the input probe intensity at the far fiber-end ($z = L$), α is the fiber loss, $g_B(\xi,\Delta\nu)$ and $I_P(\xi,\Delta\nu)$ are the respective BGS and the pump intensity at position $z = \xi$.

The existing trade-off between spatial resolution and dynamic range of the probe signal can be inferred from Eq. (1), which indicates that long sensing distances (affected by the large fiber attenuation) and high spatial resolution (short Δz) could significantly reduce the intensity contrast of the measured probe wave (ΔI_{CW}), and hence the signal-to-noise (SNR) of the measurements, thus limiting the sensing performance of long-range BOTDA sensors [2].

Moreover, it is important to mention that the best spatial resolution allowed by conventional BOTDA sensors is limited to about 1 m by the acoustic-phonon lifetime (~10 ns), since shorter pump pulses, with duration lower than ~10 ns, would induce a spectral broadening of the BGS, significantly affecting the measurement accuracy of the sensor [13]. If meter-scale spatial resolution is required by a specific application, it is possible to extend the sensing distance by using higher pump power levels; however, the onset of nonlinear effects limits the maximum pump power allowed into the sensing fiber. Actually, nonlinearities such as modulation instability (MI) and self-phase modulation (SPM) have been identified to have a detrimental impact on the sensing performance of long-range BOTDA sensors [8,9], due to the spectral broadening induced in the BGS.

Some techniques have been recently proposed [2–5] to extend the sensing distance of BOTDA sensors with meter-scale spatial resolution. For instance, optical pulse coding techniques have been proved to be very effective in enhancing the BOTDA sensing distance, as shown for example in [2] where the sensing range has been successfully extended to 50 km with 1-m spatial resolution. On the other hand, Raman amplification has been used to enhance the sensing distance up to 75 km using a first-order distributed Raman amplifier (DRA) [3] and up to 100 km using a second-order Raman pumping scheme [4], in both cases with a spatial resolution of 2 m.

In this paper we focus our attention on distributed Raman amplification to enhance the sensing range of BOTDA sensors. Even though this technique has been demonstrated to allow for interesting and promising long-range sensing distances [3–5], some issues related to the different sources of noise in DRAs have not been fully analyzed so far. Actually, the Raman pump(s) used in DRA must be properly chosen in order to fully exploit the distributed

#139361 - $15.00 USD Received 8 Dec 2010; revised 20 Jan 2011; accepted 20 Jan 2011; published 23 Feb 2011

amplification benefits, avoiding at the same time potential performance degradation in terms of electrical SNR, due to several noise sources such as polarization-dependent gain (PDG), amplified spontaneous emission (ASE), double-Rayleigh scattering (DRS), and relative intensity noise (RIN) transfer from the Raman pump(s) to the probe signal [14,15].

We present here a thorough optimization procedure, based on numerical simulations, able to identify optimum Raman-amplified BOTDA sensor parameters. Experimental results demonstrate that taking into account the many existing sources of noise [15,16], optimized conditions can be found based on bi-directional first-order Raman amplification, providing a significant sensing range enhancement with respect to previously reported BOTDA systems [3–5], achieving similar spatial and measurand resolutions.

3. Optimization of bi-directional Raman amplification for BOTDA sensors

The design of distributed Raman amplifiers for BOTDA-sensor performance improvement requires great attention in order to fully exploit the DRA benefits without incurring in the related potential penalties. In particular, the input optical power levels of the Brillouin pump, probe signal and Raman pumps need to be carefully optimized to avoid nonlinear effects [8,9] (such as MI and SPM) as well as depletion of the Brillouin pump during propagation along the sensing fiber [10,11]. Moreover, several sources of noise, potentially affecting the probe electrical SNR in DRAs, must be kept under control; among them the most important issues are related to polarization-dependent gain, double Rayleigh scattering, amplified spontaneous emission, and RIN transfer from pumps to signals [14–17]. A well-designed DRA should actually take all these effects into account and not only the gain provided by the Raman amplification process.

In this paper we optimize a bi-directional DRA for BOTDA sensing applications, taking into account all above-mentioned sources of noise. Partial differential equations describing the coupled pumps and signal evolution [14] are numerically integrated providing a powerful tool for Raman-assisted BOTDA sensors design. Considering that the Brillouin gain in BOTDA sensors is typically very low (of the order of a few percent), the Brillouin interaction can be neglected with respect to the Raman gain (which provides an ON-OFF gain of several dB) while designing the DRA [3].

Our numerical simulations are based on a fully resolved spectral model of Raman amplifiers describing the power evolution of co- and counter-propagating Raman pumps, an arbitrary number of signals, forward and backward ASE components and Rayleigh scattering effects. In compact notation, the model can be written as [14]:

$$\frac{d}{dz}P_i^{\pm}(z) = \mp\alpha_i P_i^{\pm}(z) \pm \gamma_i P_i^{\pm}(z) \pm \sum_j C_{ij} P_i^{\pm}(z)\left[P_j^{+}(z) + P_j^{-}(z)\right] \pm 2h\nu_i^{\pm}\Delta\nu \sum_j C_{ij}\left[P_j^{+}(z) + P_j^{-}(z)\right], \tag{2}$$

where the sub-indexes i and j denote the optical signals propagating at wavelengths λ_i and λ_j, respectively, $P_i^{+}(z)$ and $P_i^{-}(z)$ are the respective forward and backward propagating powers, α_i is the fiber attenuation, γ_i is the Rayleigh scattering coefficient, ν_i is the optical frequency corresponding to the wavelength λ_i, h is the Planck constant, $\Delta\nu$ is the resolution bandwidth of the ASE light, and C_{ij} is the Raman gain/depletion term between wavelengths λ_i and λ_j given by [14,16]:

$$C_{ij} = \frac{g_{ij}}{A_{eff}K_{eff}} \text{ for } \lambda_i > \lambda_j \text{ (gain term) and } C_{ij} = \frac{-g_{ij}}{A_{eff}K_{eff}}\frac{\lambda_j}{\lambda_i} \text{ for } \lambda_i < \lambda_j \text{ (depletion term),}$$

where g_{ij} is the Raman gain coefficient between wavelengths λ_i and λ_j, A_{eff} is the effective area of the fiber, and K_{eff} is the polarization factor. Note that this model allows for an accurate calculation of both signal-to-ASE-noise ratio and signal-to-DRS-noise ratio for Raman amplification performance analysis [14].

#139361 - $15.00 USD Received 8 Dec 2010; revised 20 Jan 2011; accepted 20 Jan 2011; published 23 Feb 2011

Considering that in well-designed DRA the ASE noise is expected to be the dominant noise contribution, we first carry out the design of a bi-directional DRA considering ASE and DRS noise based on the system of Eqs. (2). Then, the detrimental impact of the pump RIN transfer to the BOTDA signals (i.e. Brillouin pump and probe wave) is analyzed separately, paying special attention to the pump co-propagating with the probe signal, due to the efficient RIN transfer taking place in such a case [14,17].

Even though our design has been specifically optimized considering a Raman-amplified BOTDA sensor operating over 120 km of single-mode fiber, the procedure described here to design bi-directional DRAs is general and can also be applied for any other sensing range, as well as for other fiber types and Raman configurations, including higher-order pumping.

Considering that the effective length for Raman amplification in standard single-mode fibers is of the order of 20-25 km, we can first perform the optimization of the forward-propagating signals of the system (along + z direction) and then finalize the design considering both forward and backward directions simultaneously. The optical power of the waves launched at the fiber input (z = 0), i.e. the Brillouin pump and forward-propagating Raman pump, can be optimized considering two main design rules: *i)* the maximum power level that the Brillouin pump can reach along the sensing fiber, resulting from co-propagating Raman amplification, is limited by the onset of nonlinear effects, such as MI [8] and SPM [9]; *ii)* a proper combination of Brillouin pump and Raman co-propagating pump powers at the fiber input should be identified in order to push the maximum Brillouin pump level well inside the sensing fiber, ensuring at the same time a spatial distribution of the Brillouin pump as much uniform as possible along the sensing fiber, maximizing then the SNR of the received probe signal. Actually, the uniformity of the Brillouin pump power is an important parameter when designing a Raman-assisted BOTDA sensor; however, we have considered this effect directly on the ultimate parameter dictating the sensor performance, i.e. the attained OSNR of the probe signal, in the second stage of the optimization process (when bidirectional signal propagation is considered). In fact, the ultimate performance of the sensor is determined by the OSNR of the probe signal (impacting the electrical SNR of the measurements), which, in addition to the Brillouin and Raman gain profiles, is affected by several sources of noise.

The system of Eqs. (2) is first numerically solved, using a fourth-order Runge Kutta method, for the forward-propagating lights only (propagating along + z direction), i.e. for the Brillouin pump and the forward-propagating Raman pump. The fiber attenuation coefficient at the Raman pump wavelength (1450 nm) and at the Brillouin signals wavelength (around 1550 nm) used in the simulations were 0.28 dB/km and 0.21 dB/km, respectively. Such values, together with the other fiber parameters required to solve the mathematical model, have been obtain from experimental data resulting from fiber characterization.

Figure 1 reports a bi-dimensional contour plot showing: *i)* the output power of the Brillouin pump at 120-km distance (dotted lines), and *ii)* the maximum peak power that the Brillouin pump signal reaches along the fiber (solid lines), independently of the distance at which this level takes place. Both parameters, which have been plotted as a function of the input Brillouin pump power (x-axis) and the forward-propagating Raman pump power (y-axis), are critical in identifying optimum values on the x and y axis of Fig. 1.

#139361 - $15.00 USD Received 8 Dec 2010; revised 20 Jan 2011; accepted 20 Jan 2011; published 23 Feb 2011

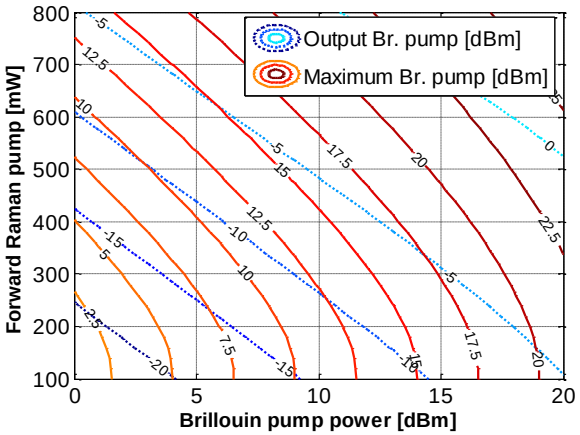

Fig. 1. Simulation results for optimization of the power level of both Brillouin and forward-propagating Raman pumps. Contour plot for output (dotted lines) and maximum (solid lines) Brillouin pump powers.

Actually, fiber nonlinearities, such as modulation instability and self-phase modulation, have been demonstrated to limit the maximum Brillouin pump power allowed into the fiber [8,9], avoiding then spectral broadening that might results in inaccuracies when measuring the BGS. The impact of such nonlinear effects on the performance of BOTDA sensors can be neglected for Brillouin pump power values below a threshold of approximately 20 dBm [8,9]. In standard BOTDA sensors this value is typically associated with the input peak power of the Brillouin pump; however, in the case of Raman-amplified BOTDA sensors, such an input power should be lowered (considering the distributed forward Raman gain) in order to ensure that the maximum Brillouin pump power, occurring at a deep location inside the fiber, does not increase beyond the onset of the above-mentioned nonlinear effects.

In our design, we have considered a power margin of ~5 dB before the onset of nonlinear effects. Figure 1 provides the allowed power values in order to ensure linear propagation regime of the Brillouin pump light. For instance, in order to keep the maximum Brillouin pump power below ~15 dBm (inside the optical fiber), an input Brillouin pump power below 10 dBm should be used (*x*-axis) together with a co-propagating Raman pump of ~400 mW (*y*-axis), resulting in an output Brillouin pump of ~-6 dBm at 120-km distance. Note that higher output Brillouin pump power can be reached by decreasing its input power and increasing the power of forward Raman pump; however, the Raman pump should be increased to high levels to provide just few dB of Raman gain, reducing the system efficiency. Moreover, such high optical power levels might not be practical due to the impact of high optical power on the reliability of the optical components, and hence, on the performance of the sensor during its lifetime.

With such an optimized condition for the Brillouin and the forward-propagating Raman pumps at the fiber input, we have then identified the best BOTDA system configuration by simulating the bi-directional Raman pumping scheme, looking for the optimum input signal probe and backward-propagating Raman pumping conditions. Figure 2 reports a bi-dimensional contour plot with the results of those simulations, where the performance of the system has been evaluated taking into account: *i)* the minimum power difference between Brillouin pump and probe along the fiber (solid lines), and *ii)* the probe optical signal-to-noise ratio (OSNR) after propagation, at $z = 0$ (dotted lines, 125-MHz bandwidth). Such two parameters allow us to maximize the OSNR, including effects of both ASE noise and DRS noise [14–16], avoiding at the same time Brillouin pump depletion [10,11]. Actually, considering that typically pump depletion effects can be neglected if the minimum power difference between the Brillouin pump and probe signal is greater than ~15 dB, then suitable power levels can be found from Fig. 2, also ensuring a sufficiently high probe OSNR.

#139361 - $15.00 USD Received 8 Dec 2010; revised 20 Jan 2011; accepted 20 Jan 2011; published 23 Feb 2011

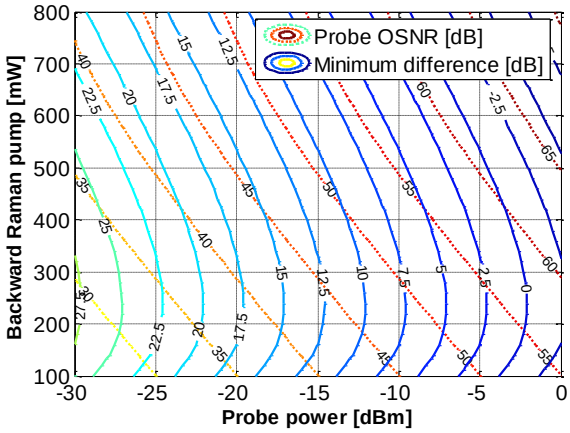

Fig. 2. Simulation results for optimization of the power level of both probe signal and backward-propagating Raman pump. Contour plot for the probe OSNR (dotted lines) and the minimum power difference between Brillouin pump and probe signals (solid lines).

A fairly optimized condition is given, for instance, by a probe power of −20 dBm together with a backward-propagating Raman pump power of 300 mW, providing a minimum Brillouin pump-probe power difference of ~17.5 dB and a resulting OSNR of ~40 dB. Note that the OSNR is computed over a 125-MHz receiver bandwidth, which is wide enough to guarantee a meter-scale spatial resolution. In addition, simulation results point out a signal-to-DRS-noise ratio greater than 55 dB, so that the total OSNR of the probe signal resulting from the bi-directional Raman amplification can be considered mainly dominated by the ASE noise. Note that such optimized parameters ensure a high sensor resolution along the whole sensing fiber. The consequent power evolution of the involved optical signals is shown in Fig. 3, where we can observe a maximum Brillouin pump power of ~14 dBm (at ~20-km distance) and a minimum Brillouin pump-probe difference of ~17.7 dB occurring at ~105-km distance, hence avoiding pump depletion and nonlinear effects.

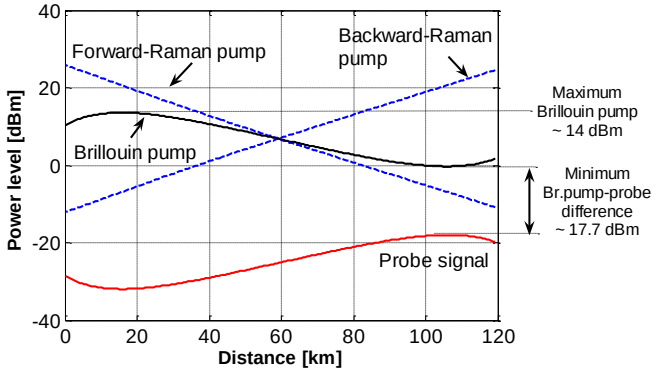

Fig. 3. Power evolution of the optimized bi-directional Raman-amplified BOTDA sensor, using the following input power levels: Brillouin pump: 10 dBm, probe signal: −20 dBm, forward-propagating Raman pump: 400 mW, and backward-propagating Raman pump: 300 mW.

Note that higher OSNR values could be achieved (while maintaining a constant Brillouin pump-probe difference, i.e. moving along a particular contour line in Fig. 2, to avoid pump depletion) by decreasing the probe input power and increasing the backward Raman pump power (in our case, moving along the line corresponding to −17.5 dB Brillouin pump-probe difference). However, such conditions can easily result in Brillouin-pump power levels well above the nonlinear threshold in proximity of the far fiber-end. Actually, simulation results have pointed out that backward-propagating Raman pump power levels higher than ~600 mW

#139361 - $15.00 USD Received 8 Dec 2010; revised 20 Jan 2011; accepted 20 Jan 2011; published 23 Feb 2011

provide exceedingly high Raman gain near the far fiber-end (>100-km distance), leading to Brillouin pump levels well above the nonlinear threshold considering the adopted margin. Such a condition can potentially induce spectral broadening of the Brillouin pump that might significantly impact on the performance of the BOTDA sensor [8,9].

An effective design of a DRA must also consider the technology that is employed for Raman pumping, which is mainly based on fiber Raman lasers (FRL) and semiconductor laser diodes (LD), such Fabry-Perot (FP) lasers. Actually, this issue has an important impact on the performance of DRAs [17], and consequently, on the sensing performance of Raman-amplified BOTDA sensors [3–5]. While semiconductor laser diodes are characterized by polarized light with relatively low power and very low RIN levels, FRLs are almost depolarized and exhibit higher power and RIN levels.

Previous experience from telecommunication applications of DRAs has clearly pointed out that the RIN transfer from the Raman pump to the signals is one of the major sources of impairments in co-propagating Raman amplification [17]. On the other hand, in the case of counter-pumped DRAs, the noise on the Raman pump is averaged over the amplifier transit time, giving rise to a low-pass transfer function characteristic with a cut-off frequency of the order of a few kHz, contrarily to co-pumping Raman schemes where the cut-off frequency of the RIN transfer function can go up to hundreds of MHz, depending on the fiber chromatic dispersion [7].

Note that the pump-to-signal RIN transfer mechanism in stimulated Brillouin scattering [18,19] is very similar to the one shown by counter-pumped Raman amplification. Therefore, due to the low cut-off frequency of the corresponding transfer function, and to the low Brillouin gain, no penalties are expected due to this effect.

In telecommunication systems the impact of the pump-to-signal RIN transfer is typically evaluated analyzing the well-known quality factor Q [7]. However, in the case of Raman-amplified BOTDA sensors, the impact of the RIN transfer can be better estimated by analyzing the degradation of the electrical SNR of the probe signal at the receiver. In the absence of RIN transfer, the electrical SNR of the probe signal can be written as:

$$SNR_S = \frac{\langle I \rangle^2}{\sigma_S^2}, \tag{3}$$

where $\langle I \rangle$ is the mean current resulting from the photo-detection of the probe signal and σ_S is the standard deviation of the noise (including for instance shot noise, thermal noise, DRS noise, and ASE noise). Considering that the noise added by RIN transfer (σ_{RIN}) can be treated as a zero-mean Gaussian random variable [7,15], the electrical SNR may be degraded to:

$$SNR_S = \frac{\langle I \rangle^2}{\sigma_S^2 + \sigma_{RIN}^2}, \tag{4}$$

where σ_{RIN} is the standard deviation of the noise resulting from the pump RIN transferred to the probe signal. This value can be obtained from the RIN-induced crosstalk (XT_{RIN}) [17] according to:

$$\sigma_{RIN}^2 = \langle I \rangle^2 \, XT_{RIN}, \tag{5}$$

where XT_{RIN} is the RIN-induced crosstalk, which can be calculated by integrating the RIN of the signal (r_S) over the receiver bandwidth between frequencies f_1 and f_2, resulting in:

$$XT_{RIN} = \int_{f_1}^{f_2} r_S(f) df. \tag{6}$$

Therefore, the noise added by the RIN transfer to the probe signal can be expressed as:

#139361 - $15.00 USD Received 8 Dec 2010; revised 20 Jan 2011; accepted 20 Jan 2011; published 23 Feb 2011

$$\sigma_{RIN}^2 = \langle I \rangle^2 \int_{f_1}^{f_2} r_S(f) df = \langle I \rangle^2 \int_{f_1}^{f_2} r_P(f) \cdot H_{RIN}(f) df, \quad (7)$$

where $r_P(f)$ represents the RIN of the pump and $H_{RIN}(f)$ is the respective RIN transfer function. Therefore, the degradation in the electrical SNR can be obtained (in dB scale) as:

$$\Delta SNR = 10 \log\left(1 + \frac{\sigma_{RIN}^2}{\sigma_S^2}\right) = 10 \log\left(1 + SNR_S \cdot XT_{RIN}\right). \quad (8)$$

The RIN transfer function can be then evaluated using the well-known expressions presented in [7] for both co- and counter-propagating pumping schemes. Figure 4 shows the spectrum of the RIN transfer functions resulting from evaluating $H_{RIN}(f)$ with standard single-mode fiber parameters (for 120-km length) and the previously designed Raman pumps, i.e. the Raman pumps propagating in forward (Fig. 4a) and backward (Fig. 4b) directions with optical power of 400 mW and 300 mW, respectively. In the forward-propagating case (Fig. 4a), the RIN transfer characteristics indicate that the pump RIN will be transferred up to a frequency of ~10 MHz (and amplified by ~10 dB) to the Brillouin pump (both propagating in the same forward direction), while the RIN transferred to the probe signal will be limited up to a few kHz. Since, in the case of BOTDA sensors with meter-scale spatial resolution, a receiver bandwidth of ~100 MHz is required, the RIN which is transferred to the counter-propagating probe signal over a few kHz bandwidth results negligible in comparison to the full receiver bandwidth.

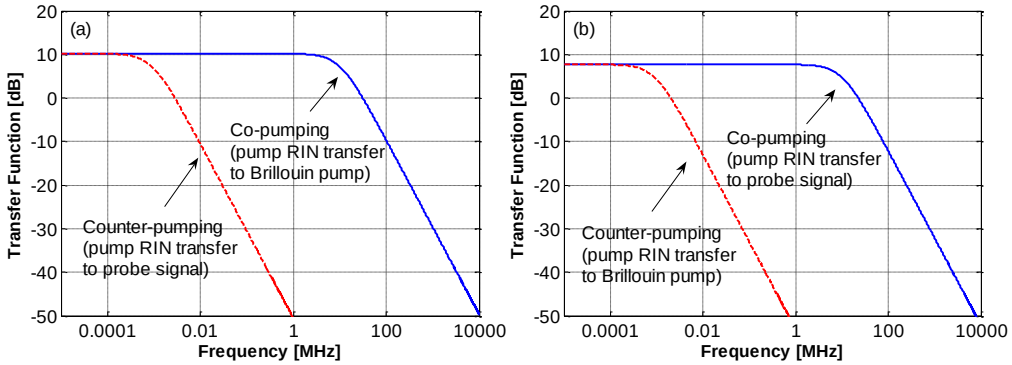

Fig. 4. Pump RIN transfer function in both co- and counter-pumping schemes, for (a) forward-propagating Raman pump, and (b) backward-propagating Raman pump.

On the other hand, we expect that the RIN of the forward-propagating Raman pump can be effectively transferred to the Brillouin pump signal over a significant bandwidth; however, the counter-propagating nature of SBS averages the noise on the fiber transit time [18,19], limiting then the impact of the RIN on the sensing performance. Consequently, the RIN transferred from the forward-propagating Raman pump can be considered negligible in the design of bi-directional Raman-amplified BOTDA sensors.

The case of Raman pump propagating in backward direction (co-propagating with the probe signal) is much more critical since its RIN can be efficiently transferred to the probe signal, as shown in Fig. 4b. Note that, since the performance of BOTDA sensors strongly depends on the electrical SNR of the probe-wave traces measured at the receiver, the degradation of the probe SNR due to RIN transfer might have a significant impact on the sensor performance. Thus, in bi-directional Raman amplification for BOTDA systems, the RIN of the backward-propagating Raman pump must be kept under control in order to avoid unwanted detrimental effects on the sensing performance.

Note that the use of higher-order Raman pumping schemes could further improve the probe OSNR at the receiver, without incurring in additional detrimental nonlinear propagation effects. However, the RIN transfer and DRS noise are also expected to increase in higher

#139361 - $15.00 USD Received 8 Dec 2010; revised 20 Jan 2011; accepted 20 Jan 2011; published 23 Feb 2011

order Raman pumping configuration [15,17], potentially cancelling out the expected benefits. Considering the physical limitation of BOTDA sensors on the spatial resolution (to 1 meter), due to the acoustic-wave response time of the order of 10 ns, the ultimate performance in terms of measurand resolution can be achieved by trading off the maximum sensing distance and the measurement time. In particular, threshold power levels for nonlinear effects and pump depletion are critical parameters that impose an ultimate limitation to the performance of the system, even when using advanced Raman pumping techniques (e.g. higher-order Raman pumping). A quantitative assessment of ultimate performance of a given system depends critically on the specific system under consideration, and involves numerical optimization stage as reported above.

4. Experimental setup

The experimental setup for the implemented BOTDA sensor based on bi-directional Raman amplification is schematically shown in Fig. 5. A distributed-feedback (DFB) laser, operating at 1550 nm with 13 dBm output power, has been used to generate both Brillouin pump and probe signals. The CW-light has been split into two branches using a 3-dB optical splitter. One of the branches is employed to generate the pulsed Brillouin pump using an Erbium-doped fiber amplifier (EDFA), a polarization controller (PC) and a Mach-Zehnder modulator (MZM). The MZM is driven by electrical pulses of 20 ns (allowing for 2-m spatial resolution) with a repetition rate of ~833 Hz (period of ~1.2 ms). Note that the location of the MZM after the EDFA allows us to filter out the inter-pulse ASE noise generated in the EDFA.

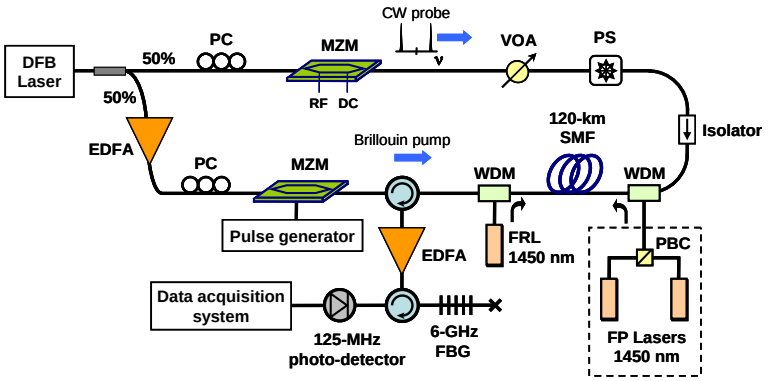

Fig. 5. Experimental setup of implemented Raman-amplified BOTDA sensor with first-order bi-directional pumping configuration.

The other branch is used to generate the probe signal using the double-sideband technique [1], where the CW-light is intensity modulated by an MZM which is controlled by a microwave (RF) signal. The optical carrier has been suppressed by properly setting the DC bias of the MZM. In order to avoid Brillouin pump depletion and nonlocal effects [10], a variable optical attenuator (VOA) has been used to adjust the probe power to −20 dBm, as indicated by the numerical simulations reported in the previous section. A polarization scrambler (PS) has been used to depolarize the probe signal, and hence, to reduce polarization-induced oscillations in the Brillouin amplification process. The Brillouin pump and probe signals are launched in counter-propagating directions along the sensing fiber through two WDM couplers, which are also used to couple both Raman pumps into the fiber. The sensing fiber is composed of two spools of 60-km single-mode fiber, allowing for a total sensing distance of 120 km.

While a depolarized FRL at 1450 nm has been used as forward-propagating Raman pump, the backward-propagating Raman pump has been implemented by multiplexing two low-RIN FP lasers (centered at 1450 nm) through a polarization beam-combiner (PBC). In this way, the impact of polarization-dependent gain of the Raman amplifier has been reduced to a negligible level. As indicated by the numerical optimization reported in Section 3, the power

#139361 - $15.00 USD Received 8 Dec 2010; revised 20 Jan 2011; accepted 20 Jan 2011; published 23 Feb 2011

of the forward-propagating Raman pump has been adjusted to 400 mW at the fiber input ($z = 0$), while the power of the backward-propagating Raman pump has been set to 300 mW at $z = L$.

At the receiver side, an additional EDFA is used as preamplifier, which is followed by an optical circulator and a 6-GHz fiber Bragg grating (FBG); this receiver scheme allows us to select the Brillouin Stokes component, while filtering out the ASE noise resulting from the bi-directional DRA and EDFA, as well as the unwanted Brillouin anti-Stokes, Rayleigh and residual carrier components. A 125-MHz photo-detector, composed of a PIN photodiode and a transimpedance amplifier (TIA), has been used together to a computer-based data acquisition system to perform the measurements.

5. Experimental results for distributed sensing

The frequency components of the BGS of the sensing fiber have been scanned by sweeping the frequency difference between the Brillouin pump and probe signal [1]. Figure 6 shows the Brillouin gain profile that has been obtained as a function of the distance (after averaging 5k traces per single scanned frequency), when using the above-optimized bi-directional DRA. We can observe that the amplitude of the BGS increases along the initial part of the sensing fiber, due to forward Raman amplification, reaching a maximum value at a distance of ~25 km. The backward-propagating Raman pump then amplifies both the Brillouin pump and probe signals near the far fiber-end (~120-km distance), leading to an enhanced Brillouin interaction at very long sensing ranges. Figure 6 also reports the Brillouin band represented by the full-width at half maximum (FWHM) of the measured BGS.

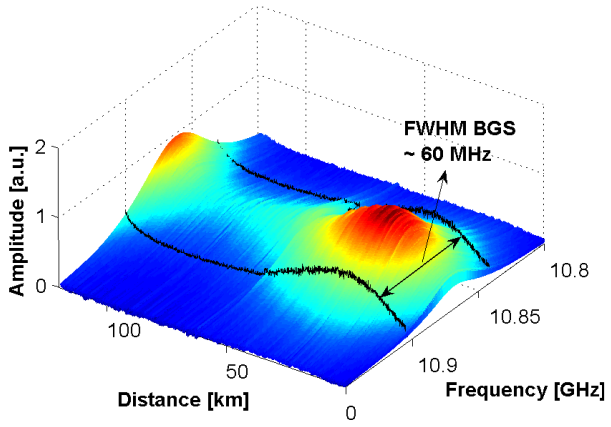

Fig. 6. Measured Brillouin gain spectrum as a function of the distance.

By fitting the measured spectrum with a Lorentzian curve at every fiber position, both the Brillouin linewidth and the BFS profile have been obtained along the fiber. Figure 7 shows the FWHM of the BGS, exhibiting a non-broadened, constant value of ~60 MHz along the whole sensing fiber. The constant behavior of the Brillouin linewidth actually confirms that our optimized bi-directional Raman amplifier enhances the BOTDA sensing range while keeping the maximum Brillouin pump power below the onset of nonlinear effects, such as MI [8] and SPM [9], avoiding then detrimental effects induced by spectral broadening [3].

#139361 - $15.00 USD Received 8 Dec 2010; revised 20 Jan 2011; accepted 20 Jan 2011; published 23 Feb 2011

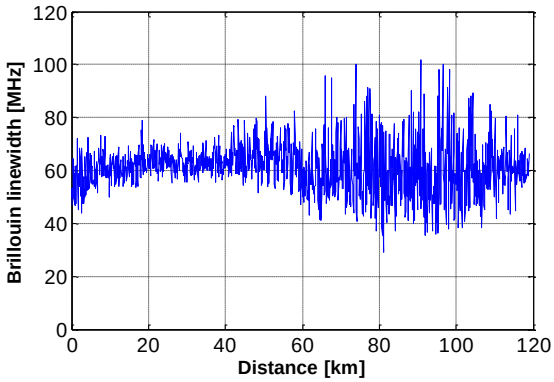

Fig. 7. Brillouin linewidth of the measured BGS as a function of the distance.

On the other hand, Fig. 8a shows the measured BFS as a function of the distance. It is important to mention that the BFS of both fiber spools are slightly different, with a variation of ~10 MHz; however, this value lies within the FWHM of the BGS, allowing for an uninterrupted SBS interaction all along the sensing fiber, and representing a realistic situation in terms of pump depletion effects if non-optimized power values were used. Note that in case pump depletion occurs, the BGS measured near the far fiber-end is expected to exhibit a spectral dip at the maximum gain around the BFS [11], potentially leading to deviations of the BFS profile along the fiber due to nonlocal effects [10]. Neither of such effects is present in our measurements (see the BFS in Fig. 8a, and the BGS near the far fiber-end in Fig. 8b), confirming that pump depletion and nonlocal effects are negligible in our experiment, as expected with the employed power values following the performed optimization.

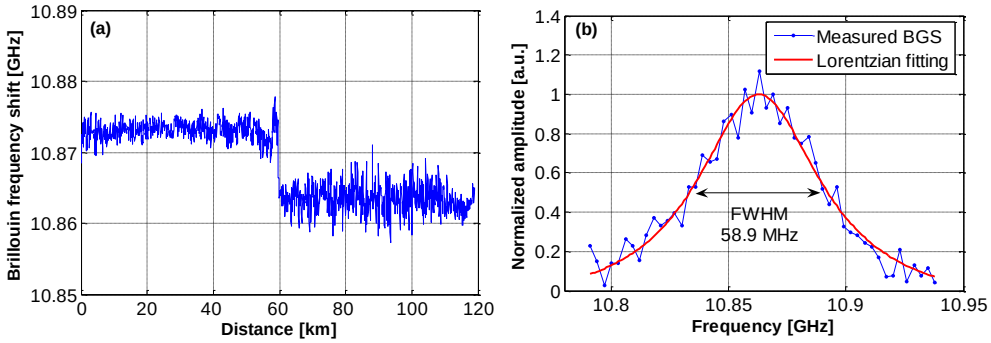

Fig. 8. (a) Brillouin frequency shift as a function of the distance. (b) Brillouin gain spectrum near 120-km distance

The measurand resolution has been then obtained by calculating the standard deviation of the measured BFS as a function of the distance. Figure 8a points out that the noisiest BFS trace segment occurs at around ~90-km distance (where the Brillouin gain is minimum), resulting in a worst resolution value of ~2.1 MHz (equivalent to 45με/2.1°C strain/temperature resolutions). Note that such a resolution is similar or better than the resolution achieved by similar Raman-amplified BOTDA sensors [3–5]; however, it can be attained over significantly larger distances. Moreover, it is important to note that such a resolution has been obtained with lower number of averaged traces compared to previously reported systems (5k averages in our case), leading to a shorter measurement time and highlighting the notable impact of bi-directional DRA optimization on the BOTDA performance. In order to further improve the measurand resolution, the number of averaged traces can be increased up to higher values, resulting in significant improved resolution.

#139361 - $15.00 USD Received 8 Dec 2010; revised 20 Jan 2011; accepted 20 Jan 2011; published 23 Feb 2011

In order to reliably assess the spatial resolution of the sensor, the detection of a short hot-spot has been verified by heating 2 m of fiber (similar to the expected spatial resolution) up to 45°C near the far fiber-end (119.337 km). The measured BGS for the last few meters of fiber is reported in Fig. 9a, showing a variation in the BFS of ~17 MHz at the hot-spot position. The room temperature at the time of the experiment was 28°C, and the measured frequency shift agrees with the expected value induced by the temperature variation of 17°C. The final temperature profile near the far fiber-end (~120-km distance) is reported in Fig. 9b, showing the location of the temperature change (~17°C variation) within ~2 m of fiber.

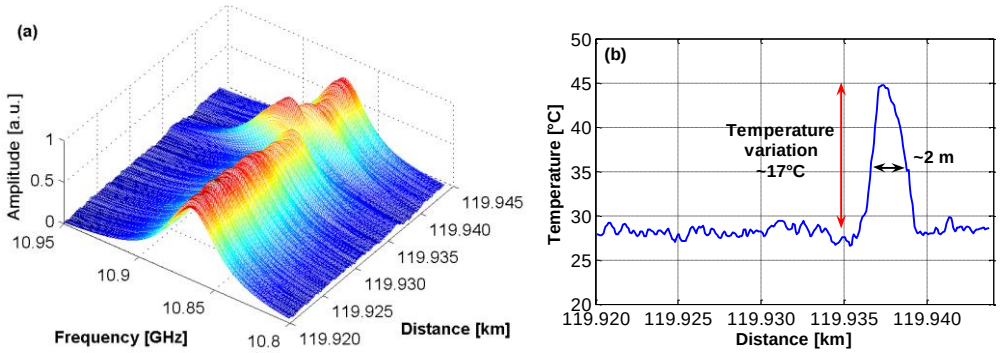

Fig. 9. Detection of a 2-m hot-spot near 120-km distance. (a) Brillouin gain spectrum and (b) temperature profile in the last 25 m of fiber (the rest of the sensing fiber is omitted for clarity)

6. Impact of pump RIN transfer on the BOTDA sensing performance

From the analysis of Section 3, we can infer that the most critical factor impacting on the sensing performance of optimized Raman-amplified BOTDA sensors is given by the RIN of the Raman pump co-propagating with the probe signal (along -z direction). For this reason an additional experimental study of the impact of RIN transfer on BOTDA sensing performance has been carried out by comparative BGS measurements employing a different type of laser (i.e. an FRL at 1450 nm) as backward-propagating Raman pump (with the same power as the previously-used polarization-multiplexed FP lasers).

Figure 10 reports the measured RIN of both pump lasers (FRL and polarization-multiplexed FP lasers) within an electrical band of 250 MHz, where we can observe the large difference in the RIN characteristics for the two lasers. By using the RIN transfer functions calculated with the optimized backward Raman pump power values [7] (shown in Fig. 4b) and the measured spectral RIN of the pump lasers shown in Fig. 10, the RIN-induced crosstalk has been calculated within the receiver bandwidth used for the experiment (125 MHz). Calculations show that, while the RIN transferred from both pump lasers to the Brillouin pump is characterized by a negligible crosstalk (–78.1 dB for the FRL and –91.6 dB for the polarization-multiplexed FP lasers), the FRL induces a significant RIN crosstalk equal to about –17.6 dB; however, the use of polarization-multiplexed FP lasers reduces the probe crosstalk down to –43.7 dB.

#139361 - $15.00 USD Received 8 Dec 2010; revised 20 Jan 2011; accepted 20 Jan 2011; published 23 Feb 2011

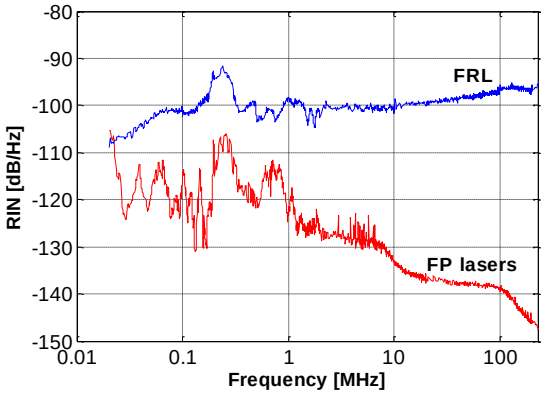

Fig. 10. Measured spectral RIN characteristics for fiber Raman laser (FRL) and polarization-multiplexed Fabry Perot (FP) lasers, respectively.

The direct impact of this RIN-induced crosstalk on the sensor performance can be observed in Fig. 11, showing the BOTDA traces measured with both pump lasers (FPL and FP lasers) at the peak of the Brillouin gain of the second fiber spool (~10.864 GHz). It can be clearly seen in Fig. 11 that the higher RIN of the FRL gives rise to a decrease in the electrical SNR of the acquired traces (about 11.5 dB SNR decrease, from direct BOTDA trace calculation). This value agrees with the one obtained from Eq. (8) based on the experimental pump RIN characterization shown in Fig. 10 and the RIN transfer functions reported in Fig. 4b, predicting an electrical SNR reduction of ~11.2 dB (as a consequence of the –17.6 dB crosstalk). This large SNR difference clearly leads to a significant reduction of the BOTDA sensor performance in terms of sensing range when high-RIN lasers (such as FRLs) are used, confirming the performance degradation observed in [3,4] due to the higher RIN values.

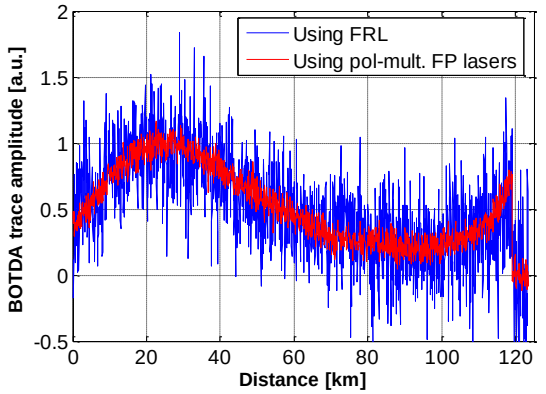

Fig. 11. Raman-amplified BOTDA traces measured near the peak Brillouin gain, using FRL and polarization-multiplexed FP lasers as backward-propagating Raman pump, respectively.

7. Conclusions

In conclusion, we have performed a thorough multi-parameter optimization of a Raman-assisted long-range BOTDA sensor with high resolution using first-order bi-directional pumping. Combining suitable power levels with the use of high-power fiber Raman lasers (FRL) and low-RIN polarization-multiplexed Fabry-Pérot (FP) lasers, operating at 1450 nm, allows us to effectively minimize the penalties linked to polarization-dependent gain, relative-intensity noise, pump depletion and nonlinear effects. In particular, experimental results have demonstrated the possibility of achieving 2-m spatial resolution throughout 120 km of single-mode fiber length with strain/temperature resolutions of 45με/2.1°C respectively.

#139361 - $15.00 USD Received 8 Dec 2010; revised 20 Jan 2011; accepted 20 Jan 2011; published 23 Feb 2011